JTTEE5 19:1179–1185
DOI: 10.1007/s11666-010-9529-5
1059-9630/$19.00 © ASM International

Mechanical Properties of $LaTi_2Al_9O_{19}$ and Thermal Cycling Behaviors of Plasma-Sprayed $LaTi_2Al_9O_{19}$/YSZ Thermal Barrier Coatings

X.Y. Xie, H.B. Guo, and S.K. Gong

(Submitted January 29, 2010; in revised form June 22, 2010)

Recently, extensive efforts have been made to develop new thermal barrier coating (TBC) materials which can operate at temperatures above 1523 K over a long term. In this article, $LaTi_2Al_9O_{19}$ (LTA) was synthesized by solid-state reaction at 1773 K, and the mechanical properties of the LTA bulk were evaluated. The microhardness is about 14 GPa, comparable to that of YSZ bulk, whereas the Young's modulus is about 44 GPa, lower than the value of YSZ. However, the fracture toughness of 0.8-1 MPa $m^{1/2}$ is much lower than that of bulk YSZ. A double-ceramic-layer LTA/YSZ TBC structure was proposed and the TBC sprayed by plasma spraying. Thermal cycling tests of the TBC specimens were performed at 1373 K with a dwell time of 10 min. The LTA remained good stability with ZrO_2 and Al_2O_3. However, the single layer LTA TBC was cracked at the LTA/bond coat interface after about 300 cycles, due to its poor thermal shock resistance, while the YSZ TBC yielded a lifetime of about 1000 cycles. The LTA/YSZ TBC remained intact even after 3000 cycles, exhibiting a promising potential as new TBC materials.

Keywords $LaTi_2Al_9O_{19}$, mechanical property, plasma spray, thermal barrier coatings (TBCs), thermal cycling

1. Introduction

The performance and efficiency of gas turbine engines are directly related to the operating temperature. Thermally sprayed thermal barrier coatings (TBCs) have been used successfully in gas turbine components to protect the metal parts from hot burner gases, leading to further increase in operating temperature and decrease of the amount of cooling air (Ref 1-3). Nowadays, state-of-the-art 7-8 wt.% yttria-stabilized zirconia (YSZ) is widely used as a standard TBC topcoat material (Ref 4-6). However, the most critical issue for YSZ is the limited operation temperature (<1473 K) for long-term application. At higher temperature, phase transformations and porous coating sintering result in cracking of the coating and increased thermal conductivity, which can accelerate the spallation failure of TBCs (Ref 7-9). Therefore, investigation of novel TBC materials with higher temperature capability, lower thermal conductivity, and longer life is one important issue for next generation turbine engines.

Some ceramic materials, such as La_2O_3-Y_2O_3-ZrO_2, Gd_2O_3-Y_2O_3-ZrO_2, $La_2Zr_2O_7$ (LZ), $La_2Ce_2O_7$ (LC), $LaMgAl_{11}O_{19}$ (LMA) and other rare earth-doped zirconia, have been investigated as potential TBC materials (Ref 10-14). Previous investigations showed good physical properties of these materials, such as lower thermal conductivity and higher thermal stability (Ref 12, 13, 15). However, the thermal expansion coefficient is often lower than that of YSZ, which leads to higher thermal stresses in the TBC system. In addition, lower toughness values are observed in these materials (Ref 12, 16). As a result, the thermal cycling properties are worse than those of YSZ coatings. A way to overcome this shortcoming is to use layered topcoats with an YSZ adjacent to the underlying bond coat (Ref 17, 18).

Recently, attention has been paid on $LaTi_2Al_9O_{19}$ (LTA) (Ref 19-21), which is featured with a huge unit cell, complex arrangement of atoms, and low symmetry. LTA reveals excellent high-temperature stability at 1773 K and low thermal conductivity. However, there is little information on the mechanical properties of LTA and the thermal cycling performances of LTA coatings so far.

In this study, LTA was synthesized by solid-state reaction, and its mechanical properties such as Young's

This article is an invited paper selected from presentations at the 4th Asian Thermal Spray Conference (ATSC 2009) and has been expanded from the original presentation. ATSC 2009 was held at Nanyang Hotel, Xi'an Jiaotong University, Xi'an, China, October 22-24, 2009, and was chaired by Chang-Jiu Li.

X.Y. Xie, H.B. Guo, and **S.K. Gong**, School of Material Science and Engineering, Beihang University, No. 37, Xueyuan Road, Beijing 100191, China and Beijing Key Laboratory for Advanced Functional Materials and China Film Technology, Beihang University, No. 37, Xueyuan Road, Beijing 100191, China. Contact e-mail: guo.hongbo@buaa.edu.cn.

modulus and fracture toughness were evaluated. LTA TBCs were produced by atmospheric plasma spraying (APS). The thermal cycling behaviors and the associated failure mechanism are investigated.

2. Experimental Procedure

2.1 Mechanical Properties of $LaTi_2Al_9O_{19}$

The LTA materials were synthesized by solid-state reaction of powders of La_2O_3 (99.99%, Grinm Rare Earth Materials Co., Ltd.), TiO_2 (≥99.7%, Shantou Xilong Chemical Company, Guangdong), and Al_2O_3 (≥99.7%, Shantou Xilong Chemical Company, Guangdong) at 1773 K for 24 h. The LTA bulk specimens for mechanical properties measurements were prepared by cold pressing of LTA powders under a pressure of 120 MPa, followed by sintering at 1873 K for 72 h. The density of the LTA bulk was determined by the Archimedes method.

Microhardness Vickers and Knoop indentations were performed on the LTA bulk using the HXZ-1000 microhardness indenter. Microhardness (H_v) was determined according to the equation:

$$H_v = 1.8544P/d^2 \quad \text{(Eq 1)}$$

where P represents the load of indent and d the length of the indent diagonal. The elastic modulus (E) was determined using the equation (Ref 22):

$$b'/a' = (b/a) - \alpha(H/E) \quad \text{(Eq 2)}$$

where b'/a' represents the indent diagonal after elastic recovery during indentation, b/a the ratio of the Knoop indenter dimensions or geometry (1/7.11), α a constant, having a value of 0.45, H the microhardness value obtained from Eq 1, and E the Young's modulus. Twenty points on the specimen were indented with a holding time of 15 s for each indentation load.

Then the LTA bulk was indented using Vickers indenter with a load of 9.8 N to produce suitable cracks, and the fracture toughness was calculated from the following equation (Ref 23):

$$K_{IC} = 0.016(E/H)^{1/2}(P/C^{3/2}) \quad \text{(Eq 3)}$$

where K_{IC} represents the fracture toughness, H the Vickers hardness, E the elastic modulus obtained from Eq 2, P the applied indentation load, and C the crack length. Scanning electron microscopy (SEM, FEI Quanta 600, the Netherlands) was used to measure the indent diagonal and crack length.

2.2 Chemical stability of LTA with Al_2O_3 and ZrO_2

In order to evaluate the chemical stability of LTA, LTA powders were mixed with Al_2O_3 powders or ZrO_2 powders in a ratio of 1:1 (in wt.%). Then the mixtures were cold-pressed into tablets, followed by sintering at 1473 K for 100 h. The phases of the mixtures were characterized by x-ray diffraction (XRD, X' Pert Pro MPD, Cu Kα radiation, the Netherlands).

2.3 Plasma Spraying and Thermal Cycling Tests of LTA TBCs

The powders for plasma-spraying LTA TBCs were produced by spray-dried method. The powders of 25-150 μm were selected for spraying LTA coatings, as shown in Fig. 1. Vacuum plasma spraying with an F4 gun was used to deposit Ni-21Co-17Cr-12Al-1Y (in wt.%) bond coats onto disk-shaped Ni-based superalloy substrate (∅ 30 × 3 mm). LTA coatings were then sprayed onto the NiCoCrAlY bond coats in an atmospheric plasma-spraying unit using a 7-M gun (Sulzer Metco). For comparison, LTA/YSZ TBC specimens and YSZ TBC specimens were also sprayed. For manufacturing of the LTA/YSZ TBC, YSZ coatings were sprayed from 204 NS powders (Sulzer Metco) as the bottom layers while LTA coatings were deposited as top layers. The processing parameters for spraying YSZ and LTA coatings are given in Table 1. It is worth noting that the sprayed coatings usually contain amorphous phase due to rapid heating and cooling during spraying. If the coating is thermally cycled in an amorphous state, then the re-crystallization together with oxidation and thermal mismatch stresses could accelerate premature spallation failure of TBC. In this context, the sprayed LTA coatings were annealed in air at 1323 K for 5 h for the re-crystallization to improve thermal cycling lifetime of TBC.

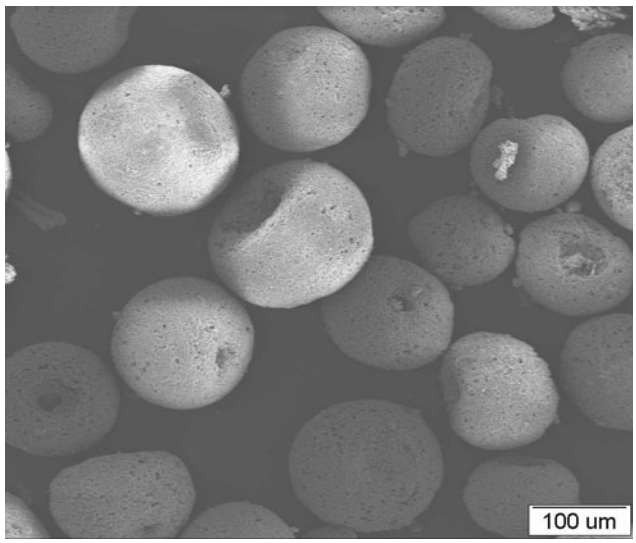

Fig. 1 Morphology of spray-dried LTA powders used for plasma spraying

Table 1 Processing parameters for plasma spraying of LTA and YSZ coating

Powder	Power, kW	Spray distance, mm	Ar, slpm	H_2, slpm	Feed rate, g/min
LTA	37.3	120	45	12	40
YSZ	38	75	38	17	35

Thermal cycling tests were performed in an air furnace by heating the specimens to 1373 K with a holding time of 10 min at the temperature, followed by compressed air cooling for 90 s. The lifetime is defined as the number of cycles at which spallation of more than 20% surface area of TBC specimens occurred.

Thermal-cycled TBC specimens were impregnated with epoxy, and then sectioned, ground, and polished. The microstructure and composition of the coatings were investigated by scanning electron microscopy (SEM) equipped with energy dispersive spectrometry (EDS, INCA Oxford, Britain), respectively.

3. Results and Discussion

3.1 Mechanical Properties of LTA Bulk

Figure 2 shows the XRD pattern of LTA powders synthesized at 1773 K for 24 h. The peaks of the synthesized LTA correspond well to those of standard $LaTi_2Al_9O_{19}$, as shown in Fig. 2(a). This indicates that single LTA phase was obtained under the synthesis condition. Decomposition and phase destabilization of the LTA bulk did not occur during sintering at 1873 K for 72 h, implying high temperature stability of LTA phase (Fig. 2c). The theoretical density of LTA is calculated to be 4.35 g/cm^3, while the relative density of the bulk samples was measured to be around 95%.

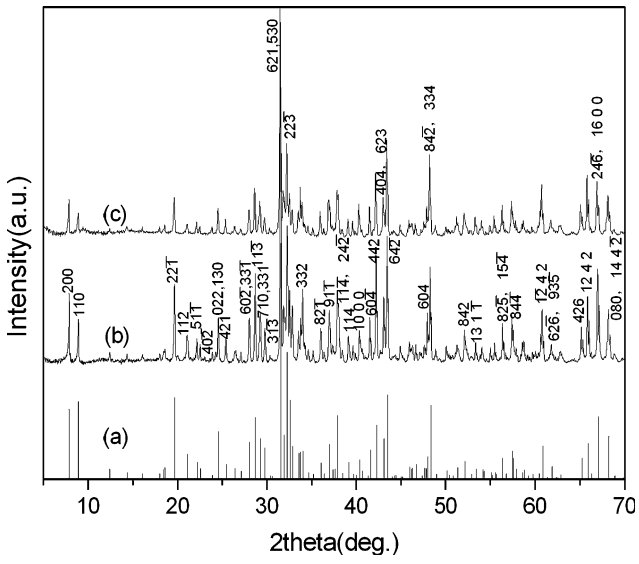

Fig. 2 XRD patterns of LTA: (a) PDF card No. 37-1233; (b) synthesized LTA powders; (c) cold-pressed LTA compact sintered at 1873 K for 72 h

The microhardness is one of the important parameters for thermal barrier coatings because the coating must withstand erosion and impingement of particles with high velocity at high temperatures. A high microhardness is desirable for TBC against erosion. The important factors that influence and determine the coating microhardness are the microstructure and porosity level. The lower the porosity level, the higher the microhardness, as well as the higher thermal conductivity and lower strain tolerance. In view of this, the optimum porosity for the typical industrial YSZ TBC is around 12%. The microhardness and the Young's modulus in this study determined by Eq 1 and 3 are given in Fig. 3. The microhardness decreased with increasing load due to the indentation size effect and approached a steady-state value at an indentation load of 200 g. At load of 500 g, crack extensions were observed. The value of hardness for LTA specimen is about 14 GPa, comparable to the value for YSZ bulk (13 ± 1 GPa, Ref 12). The value of Young's modulus E is determined to be ~44 GPa, relatively lower than that of YSZ (210 ± 10 GPa, Ref 12). The fracture toughness is in a range of 0.8-1 MPa m$^{1/2}$, significantly lower than the values of partially stabilized ZrO_2 (6-9 MPa m$^{1/2}$) (Ref 24).

It is evident that lower E is desirable for a more strain tolerant TBC. However, lower fracture toughness is not desirable for TBC because TBC tends to be cracking more easily when applying large stresses (50-100 MPa). This problem is often found in new TBC materials. The fracture toughness values of the new TBC materials are listed in Table 2. It has been shown that owing to its lower fracture toughness, the thermal cycling behavior of $La_2Zr_2O_7$ (LZ) TBC was very poor. Considering this, double-ceramic-layered (DCL) LZ/YSZ structure was

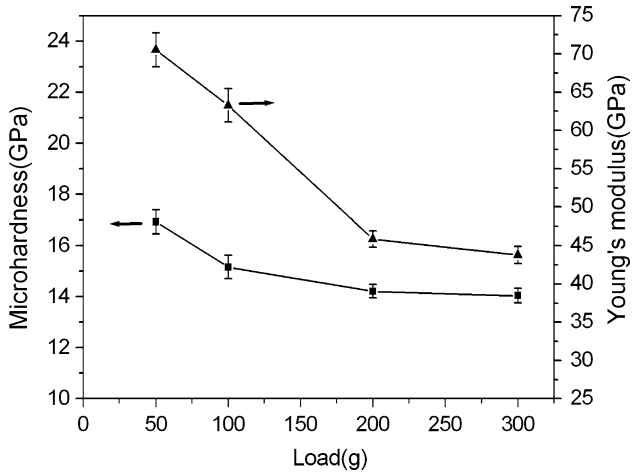

Fig. 3 Microhardness and Young's modulus of LTA bulk

Table 2 Fracture toughness values of the TBC materials

Material	YSZ (bulk)	YSZ (coating)	LMA (bulk)	LZ (bulk)	LC (coating)
State	Dense	Porosity: 12%	Density: ~97%	Density: >95%	
Toughness, MPa m$^{1/2}$	6-9 (Ref 24)	1-3 (Ref 1, 12, 25)	5.25 (Ref 26)	1.1 (Ref 12)	1.3-1.5 (Ref 16)

proposed, and it proved to be effective in improving the thermal cycling lifetime (Ref 17, 27, 28). This suggests that the DCL structure could be adopted in this study, in which LTA with high temperature capability is used as the top layer while YSZ with good mechanical properties forms the bottom layer.

3.2 Chemical Stability of LTA

As thermal barrier materials, LTA must maintain good chemical stability with other parts such as the thermally grown oxide (TGO) in TBC system during high-temperature exposure, to achieve a long service lifetime. It has been shown that $La_2Ce_2O_7$ (LC) TBC reacted with TGO mainly comprising alumina during thermal cycling. In order to solve this problem, YSZ was used as an interlayer between the LC top layer and TGO (Ref 18). On the other hand, YSZ is usually considered as the bottom layer in the DCL TBC system because of its satisfactory mechanical properties such as thermal expansion and fracture toughness (Ref 29). Considering this, it makes sense to evaluate the chemical stability of LTA in a thermal barrier coating system.

Figure 4(a) shows the XRD patterns of the compact of the mixture of LTA and α-Al_2O_3 after 100-h heat treatment at 1473 K. No other phases except LTA and α-Al_2O_3 are identified in the compact. Also no chemical reaction between LTA and ZrO_2, after 100-h heat treatment at 1473 K is found in XRD results (Fig. 4b). Therefore, it can be concluded that LTA remained in good chemical compatibility while being in contact with ZrO_2 and Al_2O_3 at 1473 K.

3.3 Plasma Spraying of LTA TBCs

Owing to the good chemical stability of LTA with ZrO_2, a LTA/YSZ DCL TBC structure was designed. An YSZ layer was sprayed onto the bond coat as the bottom layer, and a LTA layer was sprayed as the top layer. The DLC coating with the YSZ layer of ~80 μm thickness and the LTA layer of ~200 μm thickness showed the most promising thermal cycling performance. Therefore, the LTA/YSZ coating structure was optimized. For comparison, single-layered LTA TBC specimens are also prepared.

The microstructure of cross-section of plasma-sprayed LTA TBC is shown in Fig. 5. The LTA coating has a thickness of ~200 μm, intimately bonding to the underlying bond coat. The porosity is measured by mercury porosimetry to be around 8%. Figure 6 shows the XRD patterns of the coatings before and after 5 h heat-treatment at 1323 K. Amorphous phase was formed in the sprayed coating due to rapid cooling of the LTA coating during plasma spraying processing. After heat-treatment, the crystallization of the coating occurred only partially, since the peaks of the LTA phase are rather broad. This indicates that the temperature and dwell time are

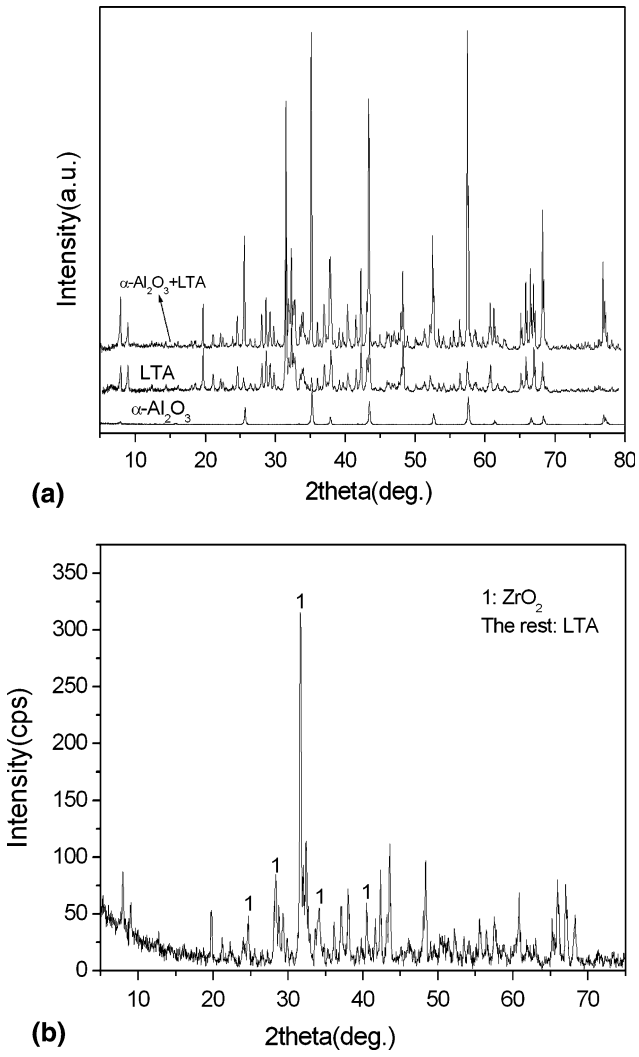

Fig. 4 XRD patterns of the bulk cold-pressed from: (a) the mixture of 50 wt.% LTA powders and Al_2O_3 powders; (b) the mixture of 50 wt.% LTA powders and ZrO_2 powders, followed by heat-treatment at 1473 K for 100 h

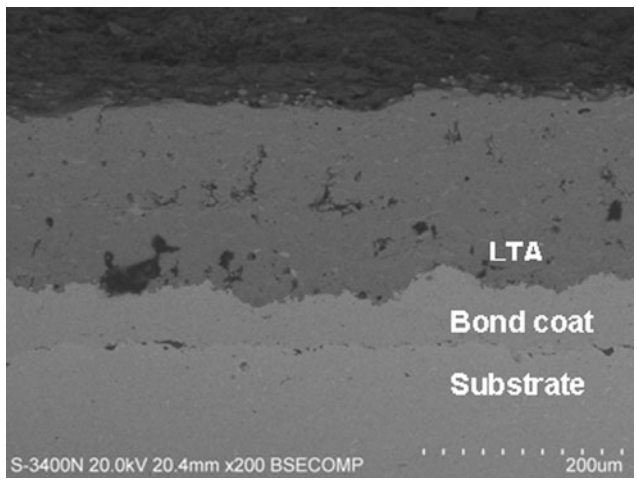

Fig. 5 SEM micrograph of cross-section of plasma-sprayed LTA TBC

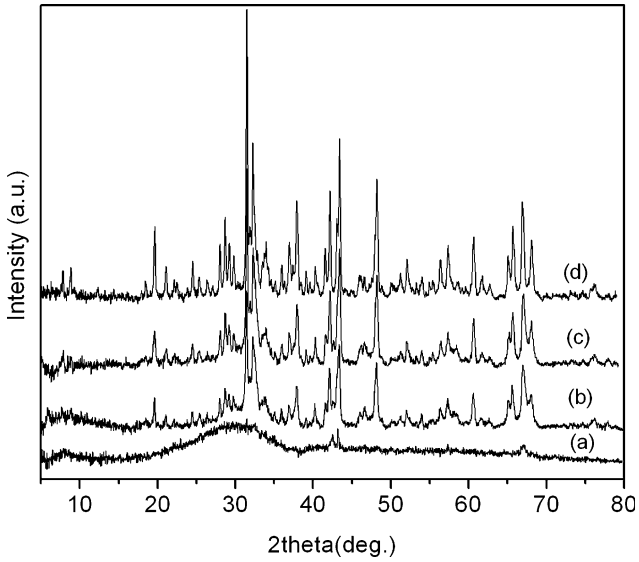

Fig. 6 XRD patterns of the LTA coatings: (a) as-sprayed; (b) 5-h heat treatment at 1323 K; (c) 300 thermal cycles; (d) 3000 thermal cycles

insufficient to complete the crystallization. The chemical composition of LTA coating was analyzed by EDS to be: La: 3.7, Ti: 7.0, Al: 26.7, O: bal. (in at.%). The atom ratio of La:Ti:Al:O is nearly 1:2:9:19, close to the stoichiometric composition of $LaTi_2Al_9O_{19}$. Therefore, it can be concluded that the LTA coating with nearly stoichiometric composition was obtained for the used plasma spraying conditions.

3.4 Thermal Cycling Behaviors of LTA TBCs

Spallation failure of the single LTA TBC specimen was observed after about 300 cycles (nearly 50 h thermal exposure at 1373 K), as shown in Fig. 7(a). The microstructure of the failed LTA coating is shown in Fig. 7(b). The TBC was cracked at the interface between the LTA topcoat and NiCoCrAlY bond coat. The TGO layer formed on the bond coat is rather thin, implying that oxidation of the bond coat is not the major factor governing failure. As LTA showed a good stability with Al_2O_3, reactions with TGO might be excluded. One of the possible reasons for the premature failure of the LTA TBC could be the larger thermal stress generated during thermal cycling due to thermal expansion mismatch between LTA coating and superalloy substrate. In our previous study, it has been shown that the TECs for LTA range from 8.5×10^{-6} to 11×10^{-6} K^{-1}, which are comparable to those for YSZ. Probably the relatively low fracture toughness of LTA coating promotes crack growth under thermal cycling.

Compared to the LTA TBC specimen, the YSZ TBC specimen exhibited a longer lifetime of around 1000 cycles. Figure 8 shows the micrographs of cross sections of the failed YSZ TBC. Delamination is observed (Fig. 8a) mainly within the YSZ near the YSZ/TGO interface. The high magnification image in Fig. 8(b) shows

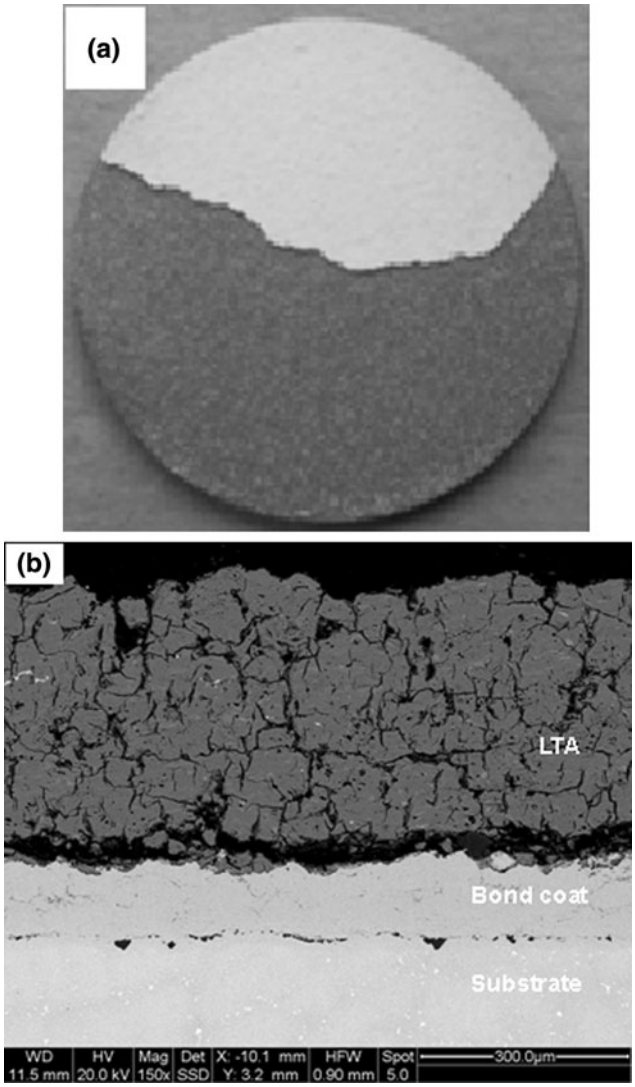

Fig. 7 Photograph (a) and SEM micrograph of cross-section (b) of LTA TBC after 300 cycles at 1373 K

a crack in TGO layer. The average thickness of TGO is ~5 μm. These cracks may be caused by the tensile stresses created at the imperfections by the growth of the TGO, in agreement with the failure mechanism studied by many investigators (Ref 30). On the contrary, for the LTA/YSZ DCL TBC specimen, no coating spallation was observed after 3000 cycles, as shown in Fig. 9(a). Figure 9(b) shows the micrograph of cross section of the TBC specimen after 3000 cycles (nearly 500-h thermal exposure at 1373 K). The LTA/YSZ coating was still intimately bonded to the underlying bond coat. Figure 9(c) is a high magnification image showing the good bonding at LTA/YSZ, YSZ/TGO and TGO/bond coat interfaces. The thickness of the TGO layer is much thicker than that of the single LTA TBC, due to its longer thermal exposure. The XRD pattern of LTA/YSZ TBC after 3000 thermal cycles is shown in Fig. 6(d). No decomposition and phase destabilization of LTA coating occurred, revealing good phase stability.

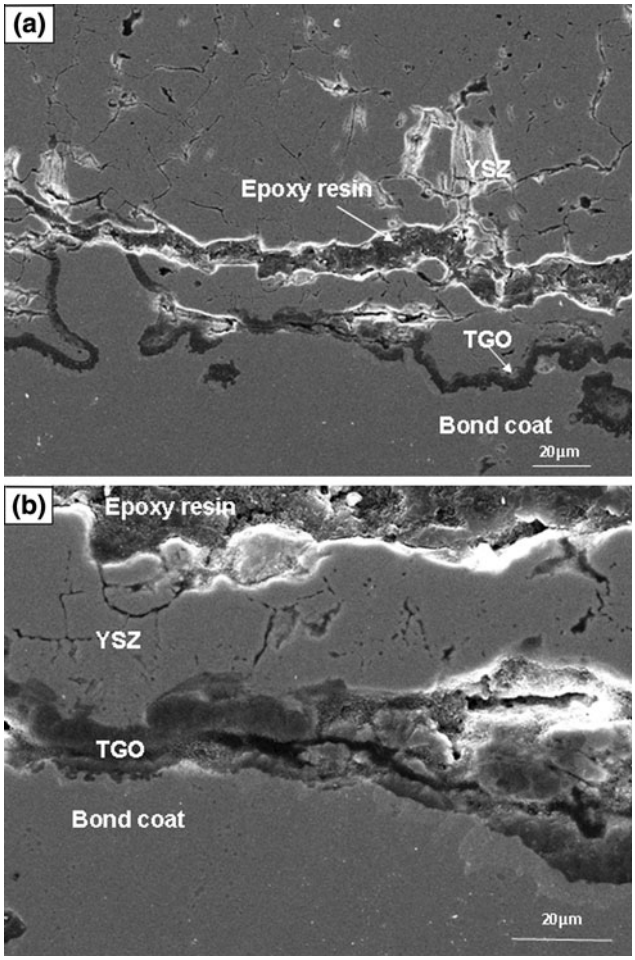

Fig. 8 (a) SEM micrograph of cross section of YSZ TBC after 1000 cycles at 1373 K; (b) high magnification image at the YSZ/TGO interface

The LTA/YSZ TBC has also survived thousands of cycles in a burner rig testing at a coating surface temperature of higher than 1573 K, exhibiting a very promising potential as a novel TBC materials. The double ceramic layer coatings have been proved to be an effective way to extend the thermal cycling lifetime.

4. Conclusions

Single phase of $LaTi_2Al_9O_{19}$ was synthesized by solid-state reaction of La_2O_3, TiO_2 and Al_2O_3 at 1773 K for 24 h. The microhardness of the LTA bulk is about 14 GPa, comparable to that of the YSZ bulk, whereas the Young's modulus is about 44 GPa, relatively lower than that of YSZ. However, its fracture toughness is of the order of 0.8-1 MPa $m^{1/2}$, much lower than that of YSZ bulk. A double-ceramic-layer LTA/YSZ TBC was sprayed by plasma spraying. The LTA remained in good stability with ZrO_2 and Al_2O_3. Thermal cycling results showed that the LTA TBC failed at the LTA/bond coat interface after

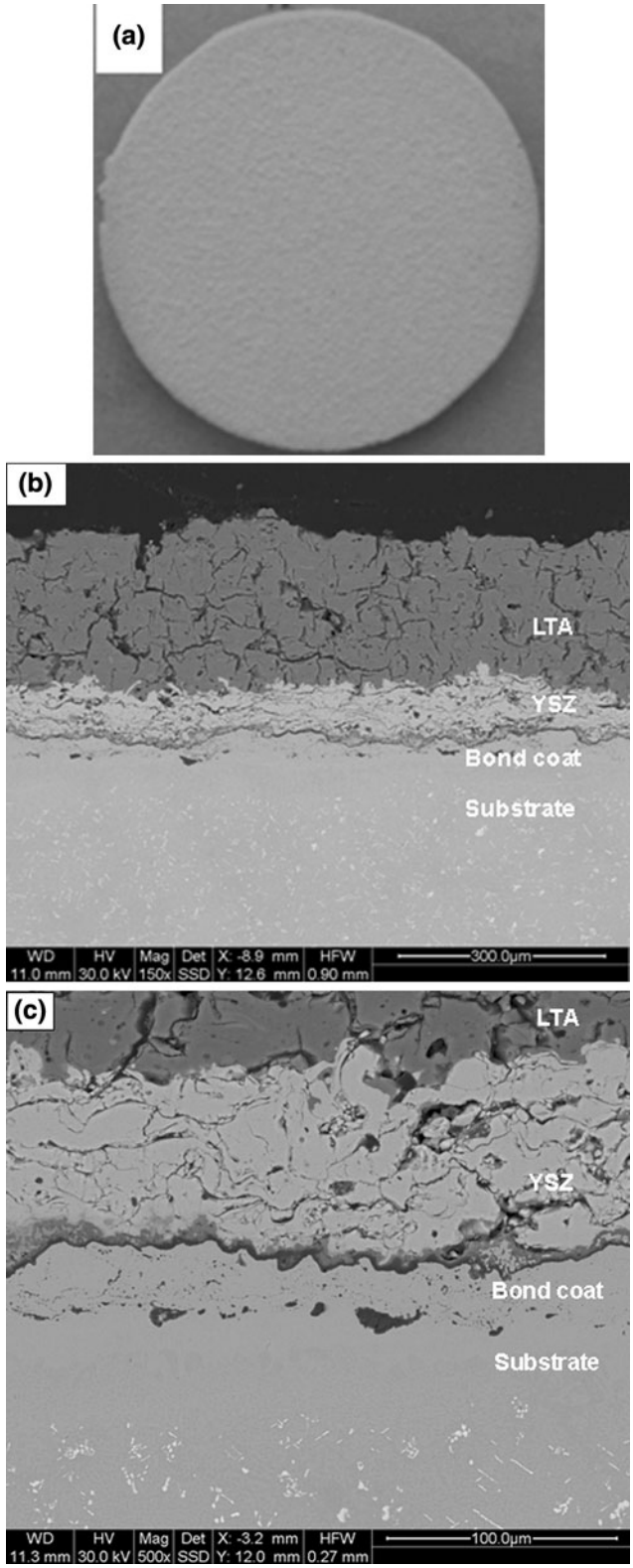

Fig. 9 (a) Photograph of LTA/YSZ double-ceramic-layered TBC after 3000 cycles at 1373 K; (b) SEM micrograph of cross section and (c) higher resolution micrograph of bond coat/YSZ interface of LTA/YSZ double ceramic layered TBC after 3000 cycles at 1373 K

around 300 cycles at 1373 K possibly due to its lower fracture toughness, while the YSZ TBC yielded a lifetime of around 1000 cycles. The LTA/YSZ TBC remained intact even after 3000 cycles, indicating a promising potential as new TBC materials.

Acknowledgments

The research is sponsored by National Natural Science Foundation of China (NSFC, Nos. 50771009 and 50731001).

References

1. R. Taylor, J.R. Brandon, and P. Morrell, Microstructure Composition and Property Relationships of Plasma-Sprayed Thermal Barrier Coatings, *Surf. Coat. Technol.*, 1992, **50**(2), p 141-149
2. R.A. Miller, Current Status of Thermal Barrier Coatings—An Overview, *Surf. Coat. Technol.*, 1987, **30**(1), p 1-11
3. N.P. Padture, M. Gell, and E.H. Jordan, Thermal Barrier Coatings for Gas-Turbine Engine Applications, *Science*, 2002, **296**, p 280-284
4. W.A. Nelson and R.M. Orenstein, TBC Experience in Land-Based Gas Turbines, *J. Therm. Spray Technol.*, 1997, **6**(2), p 176-180
5. S. Stecura, Optimization of the Ni-Cr-Al-Y/ZrO_2-Y_2O_3 Thermal Barrier System, *Adv. Ceram. Mater.*, 1986, **1**(1), p 68-76
6. S. Bose and J. DeMasi-Marcin, Thermal Barrier Coating Experience in Gas Turbine Engines at Pratt & Whitney, *J. Therm. Spray Technol.*, 1997, **6**(1), p 99-104
7. F. Cernuschi, P. Bianchi, M. Leoni, and P. Scardi, Thermal Diffusivity/Microstructure Relationship in Y-PSZ Thermal Barrier Coatings, *J. Therm. Spray Technol.*, 1999, **8**(1), p 102-109
8. J. Ilavsky and J.K. Stalick, Phase Composition and Its Changes During Annealing of Plasma-Sprayed YSZ, *Surf. Coat. Technol.*, 2000, **127**(2-3), p 120-129
9. U. Schulz, Phase Transformation in EB-PVD Yttria Partially Stabilized Zirconia Thermal Barrier Coatings During Annealing, *J. Am. Ceram. Soc.*, 2000, **83**(4), p 904-910
10. M. Matsumoto, N. Yamaguchi, and H. Matsubara, Low Thermal Conductivity and High Temperature Stability of ZrO_2-Y_2O_3-La_2O_3 Coatings Produced by Electron Beam PVD, *Scr. Mater.*, 2004, **50**, p 867-871
11. M.N. Rahaman, J.R. Gross, R.E. Dutton, and H. Wang, Phase Stability, Sintering, and Thermal Conductivity of Plasma-Sprayed ZrO_2-Gd_2O_3 Compositions for Potential Thermal Barrier Coating Applications, *Acta Mater.*, 2006, **54**(6), p 1615-1621
12. R. Vassen, X. Cao, F. Tietz, D. Basu, and D. Stöver, Zirconates as New Materials for Thermal Barrier Coatings, *J. Am. Ceram. Soc.*, 2000, **83**(8), p 2023-2028
13. X. Cao, R. Vassen, W. Fischer, F. Tietz, W. Jungen, and D. Stöver, Lanthanum-Cerium Oxide as a Thermal Barrier-Coating Material for High-Temperature Applications, *Adv. Mater.*, 2003, **17**, p 1438-1442
14. C. Friedrich, R. Gadow, and T. Schirmer, Lanthanum Hexaaluminate—A New Material for Atmospheric Plasma Spraying of Advanced Thermal Barrier Coatings, *J. Therm. Spray Technol.*, 2001, **10**, p 592-598
15. H. Lehmann, D. Pitzer, G. Pracht, R. Vaßen, and D. Stöver, Thermal Conductivity and Thermal Expansion Coefficients of the Lanthanum Rare-Earth-Element Zirconate System, *J. Am. Ceram. Soc.*, 2003, **86**(8), p 1338-1344
16. Y. Wang, H.B. Guo, and S.K. Gong, Thermal Shock Resistance and Mechanical Properties of $La_2Ce_2O_7$ Thermal Barrier Coatings with Segmented Structure, *J. Therm. Spray Technol.*, 2009, **35**(7), p 2639-2644
17. R. Vaßen and D. Stöver, New Thermal Barrier Coatings Based on Pyrochlore/YSZ Double Layer System, *Int. J. Appl. Ceram. Technol.*, 2005, **1**, p 351-361
18. W. Ma, S.K. Gong, H.F. Li, and H.B. Xu, Novel Thermal Barrier Coatings Based on $La_2Ce_2O_7$/8YSZ Double-Ceramic-Layer Systems Deposited by Electron Beam Physical Vapor Deposition, *Surf. Coat. Technol.*, 2008, **202**, p 2704-2708
19. H.B. Guo, X.Y. Xie, H.B. Xu, and S.K. Gong, Manufacturing of Thermal Barrier Coating with Column Structure Ceramic Layer, China Patent No. ZL200710118236.5, 16 Sept 2009
20. S.K. Gong, X.Y. Xie, H.B. Guo, and H.B. Xu, Synthesis of $LaTi_2Al_9O_{19}$ by Sol-gel Method, China Patent No. ZL200810101373.2, 2 Jun 2010
21. H.B. Xu, X.Y. Xie, H.B. Guo, and S.K. Gong, Synthesis of $LaTi_2Al_9O_{19}$ by Co-precipitation Method, China Patent No. ZL200810101374.7, 22 Jan 2010
22. D.B. Marshall, T. Noma, and A.G. Evans, A Simple Method for Determining Elastic-Modulus-to-Hardness Ratio using Knoop Indentation Measurements, *J. Am. Ceram. Soc.*, 1982, **65**(10), p c175-c176
23. G.R. Anstis, P. Chantikul, B.R. Lawn, and D.B. Marshall, A Critical Evaluation of Indentation Techniques for Measuring Fracture Toughness: 1. Direct Crack Measurements, *J. Am. Ceram. Soc.*, 1981, **64**(9), p 533-538
24. T.K. Gupta, Role of Stress-Induced Phase Transformation in Enhancing Strength and Toughness of in Zirconia Ceramics, *Fracture Mechanics of Ceramics*, Vol 4, R.C. Bradt, D.P.H. Hasselman, and F.F. Lange, Ed., Plenum Press, 1977, p 877-889
25. G.K. Beshish, C.W. Florey, F.J. Worzala, and W.J. Lenling, Fracture Toughness of Thermal Spray Ceramic Coatings Determined by the Indentation Technique, *J. Therm. Spray Technol.*, 1993, **2**(1), p 35-38
26. Y. Zhang, Q. Li, X. Ma, and X. Cao, Synthesis and High-pressure Sintering of Lanthanum Magnesium Hexaaluminate, *Mater. Lett.*, 2008, **62**, p 923-925
27. Z. Xu, L. He, R. Mu, X. Zhong, Y. Zhang, J. Zhang, and X. Cao, Double-Ceramic-Layer Thermal Barrier Coatings of $La_2Zr_2O_7$/YSZ Deposited by Electron Beam-Physical Vapor Deposition, *J. Alloy Compd.*, 2009, **473**, p 509-515
28. R. Vaßen, X. Cao, and D. Stöver, Improvement of New Thermal Barrier Coating Systems Using a Layered or Graded Structure, *Ceram. Eng. Sci. Proc.*, 2001, **22**(4), p 435-442
29. C. Mercer, J.R. Williams, D.R. Clarke, and A.G. Evans, On a Ferroelastic Mechanism Governing the Toughness of Metastable Tetragonal-Prime (t′) Yttria-Stabilized Zirconia, *Proc. R. Soc.*, 2007, **463**, p 1393-1408
30. A. Rabiei and A.G. Evans, Failure Mechanisms Associated with the Thermally Grown Oxide in Plasma-Sprayed Thermal Barrier Coatings, *Acta Mater.*, 2000, **48**(15), p 3963-3976